J. Membrane Biol. 181, 91–105 (2001)
DOI: 10.1007/s00232-001-0013-5

The Journal of
Membrane
Biology

IP_3-Gated Channels and their Occurrence Relative to CNG Channels in the Soma and Dendritic Knob of Rat Olfactory Receptor Neurons

R. Kaur, X.O. Zhu, A.J. Moorhouse, P.H. Barry
School of Physiology and Pharmacology, The University of New South Wales, Sydney 2052, Australia

Received: 3 October 2000/Revised: 29 January 2001

Abstract. Olfactory receptor neurons respond to odorants with G protein-mediated increases in the concentrations of cyclic adenosine 3′,5′-monophosphate (cAMP) and/or inositol-1,4,5-trisphosphate (IP_3). This study provides evidence that both second messengers can directly activate distinct ion channels in excised inside-out patches from the dendritic knob and soma membrane of rat olfactory receptor neurons (ORNs). The IP_3-gated channels in the dendritic knob and soma membranes could be classified into two types, with conductances of 40 ± 7 pS ($n = 5$) and 14 ± 3 pS ($n = 4$), with the former having longer open dwell times. Estimated values of the densities of both channels from the same inside-out membrane patches were very much smaller for IP_3-gated than for CNG channels. For example, in the dendritic knob membrane there were about 1000 CNG channels $\cdot \mu m^{-2}$ compared to about 85 IP_3-gated channels $\cdot \mu m^{-2}$. Furthermore, only about 36% of the dendritic knob patches responded to IP_3, whereas 83% of the same patches responded to cAMP. In the soma, both channel densities were lower, with the CNG channel density again being larger (~57 channels $\cdot \mu m^{-2}$) than that of the IP_3-gated channels (~13 channels $\cdot \mu m^{-2}$), with again a much smaller fraction of patches responding to IP_3 than to cAMP. These results were consistent with other evidence suggesting that the cAMP-pathway dominates the IP_3 pathway in mammalian olfactory transduction.

Key words: cAMP — Single channels — Patch clamp — Olfactory transduction

Introduction

Odorants bind to specialized G protein-coupled receptor proteins that are members of a large multi-gene family (Buck & Axel, 1991) located on the plasma membrane of cilia extending from the dendrite of olfactory receptor neurons (ORNs) into the mucus layer covering the olfactory epithelium. Figure 1 shows a schematic diagram of possible odorant-receptor interactions resulting in G protein-mediated activation of adenylate cyclase or phospholipase C, leading to an elevation in the levels of the second messengers, adenosine 3′,5′-cyclic monophosphate (cAMP) or inositol-1,4,5 trisphosphate (IP_3) respectively, as also reported by various groups (e.g., Huque & Bruch, 1986; Breer, Boekhoff & Tareilus, 1990; Balasubramanian, Lynch & Barry, 1996). Following the elevation of cAMP or IP_3, ion channels directly and indirectly gated by these second messengers are opened in the olfactory cilia membrane. The contribution of cAMP to an odorant response has been much more clearly established than that of IP_3 and it has been suggested from work in amphibia (Kurahashi & Yau, 1993) and rat (Lowe & Gold, 1993a, b) that an increase in cAMP concentration elicited in olfactory neurons by some odorants directly causes the opening of nonspecific cation channels. They suggested that the initial olfactory receptor response is a mixture of two currents, Na^+ and Ca^{2+} entering through the cAMP-gated channels, which would tend to depolarize the ORNs. It has also been shown that cAMP-gated channels are mainly localized in the olfactory cilia (Kurahashi & Kaneko, 1991; 1993), although channels are also found at a very high density on the dendritic knobs and to a lesser extent on the soma of mammalian ORNs (Balasubramanian, Lynch & Barry, 1995). The entering Ca^{2+} is then considered to go on and activate a secondary Cl^- current, which will further increase depolarization and aid in the initiation of the action potential (Kleene & Gestland, 1991; Kleene, 1993; Kurahashi & Yau, 1993; Lowe & Gold, 1993a). Since no Ca^{2+} stores are apparent in the outer dendrites of rat ORNs, it is assumed that a second messenger-dependent Ca^{2+}-influx starts the olfactory transduction cascade

Correspondence to: P.H. Barry

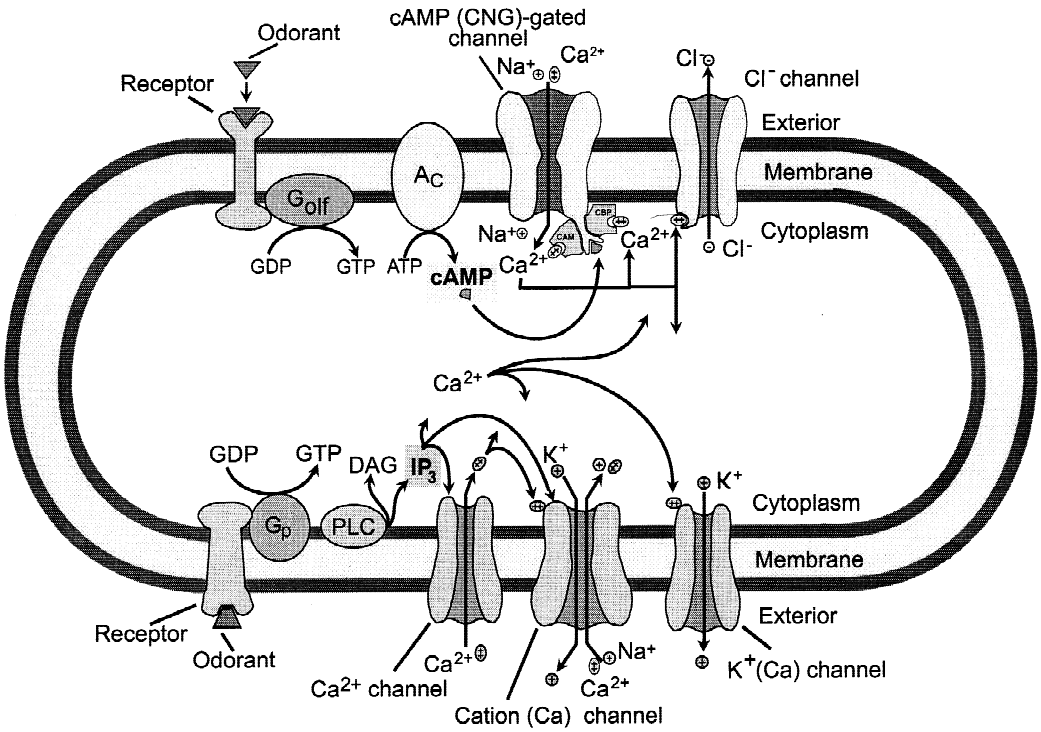

Fig. 1. A schematic diagram depicting olfactory transduction involving the cAMP and IP_3 pathways. The upper part shows the cAMP pathway: the binding of certain odorants to olfactory receptors activates G-protein-mediated formation of intracellular cAMP. The subsequent elevation of the cAMP concentration directly causes the opening of cAMP-gated channels, which further mediates an influx of Ca^{2+}, eliciting an increase in $[Ca^{2+}]_i$, that causes an opening of Ca^{2+}-activated Cl^- channels. The lower half shows the IP_3 pathways: some odorants stimulate G-protein-mediated formation of IP_3. The increase in intracellular IP_3 causes the opening of a Ca^{2+}-permeable conductance and a nonspecific cation conductance. The influx in Ca^{2+} elicits an increase in $[Ca^{2+}]_i$, which also opens a nonspecific cation conductance and may also activate Ca^{2+}-activated K^+ channels. Modified from Fig. 9 of Balasubramanian et al. (1996) and Fig. 1 (B&C) of Restrepo et al. (1996).

(Breer et al., 1990). This channel activity can also elicit changes in the frequency of firing of action potentials in the receptor cell axons, thereby conveying further olfactory information to the CNS (e.g., Lowe & Gold, 1993a; Schild & Restrepo, 1998).

Restrepo et al. (1990) first postulated that IP_3 also mediated odorant-induced depolarization of the plasma membrane of catfish olfactory cilia via the direct opening of IP_3-gated cation channels. At this time, Breer et al. (1990) suggested that both second messengers were necessary and that they mediated different odorant-specific transduction pathways. For example, odorants that elevate IP_3 in ciliary membrane preparations of rat ORNs failed to elevate cAMP and vice-versa for cAMP odorants and IP_3 elevation (Breer et al., 1990). Since then, considerable evidence that IP_3 can also gate and modulate ion channels in the olfactory cilia membrane has been reported in many other nonmammalian species such as lobster (Fadool & Ache, 1992), salamander (Firestein, Zufall & Shepherd, 1991), catfish (Goulding et al., 1992; *see also* Kalinoski et al., 1992), *Xenopus laevis* (Schild, Lischka & Restrepo, 1995), bullfrog (Suzuki, 1994) and frog (Kashiwayanagi, 1996). It was suggested that activation of these IP_3-gated channels elicited depolarization of the ORN membrane potential. More recently, both IP_3 and cAMP transduction pathways have been reported in lobster and amphibian ORNs, where odorants have been shown to suppress, as well as excite, the cells via separate conductances (Miyamoto et al., 1992; Boekhoff et al., 1994; Schild & Restrepo, 1998).

However, evidence for IP_3-mediated olfactory transduction even in non-mammalian species has not always been consistent. For example, several laboratories have failed to obtain responses upon dialysis of IP_3 into the cytoplasm of salamander olfactory receptor neurons (Firestein et al., 1991; Lowe & Gold, 1993a). In addition, two laboratories have reported no effect with IP_3 on currents recorded in excised patches from frog olfactory cilia membranes (Kleene, Gesteland & Bryant, 1994; Nakamura et al., 1996).

On the other hand, in mammalian species, the role of IP_3 in olfactory signaling transduction has been very controversial. Brunet, Gold & Ngai (1996) and Belluscio et al. (1998) reported that in mice with a CNG channel knockout or a G_{olf} knockout mutation (with G_{olf} linking odorant-receptor binding to cAMP formation via stimu-

lation of adenylate cyclase), the mice failed to respond to a wide array of odorants known to activate either cAMP or IP_3 pathways, suggesting that the cAMP serves as the sole second messenger mediating excitatory olfactory signal transduction. Gold (1999) therefore concluded that the cAMP mechanism is the sole excitatory transduction mechanism in vertebrate olfactory receptor cells. In spite of these experiments, Okada et al. (1994) and Lischka et al. (1999) have now provided evidence for IP_3-gated channels in rat olfactory receptor neurons (ORNs).

The aim of our paper was therefore twofold. First, to further confirm and investigate the presence and properties of the IP_3 signalling pathway in mammalian ORNs. Second, if their presence was confirmed, to estimate the relative densities of cAMP- and IP_3-gated channels in membrane patches from these ORNs, with a view to being able to make some inferences about their relative contributions to olfactory transduction in such cells. The intention was to measure channel densities of both second messenger-gated channels in patches from both the dendritic knob and soma of acutely dissociated rat ORNs. Some of the results have been published in abstract form (Kaur, Moorhouse & Barry, 1999).

Materials and Methods

Cell Preparation

Enzymatically dissociated olfactory receptor neurons from adult female Wistar rats were obtained from olfactory epithelial tissue lining the septum and turbinates. Cell dissociation and isolation techniques were basically the same as those described previously (e.g., Lynch & Barry, 1991). Olfactory receptor neurons were enzymatically dissociated by incubating the olfactory epithelial tissue pieces in divalent cation-free Dulbecco's phosphate-buffered saline (DPBS) containing 0.2 mg/ml trypsin (Calbiochem, La Jolla, CA) for 27 min at 37°C. The dissociation was terminated by removing the dissociation solution and replacing it with 10 ml of General Mammalian Ringer's solution (GMR) to which 0.1 mg of trypsin inhibitor (Calbiochem, La Jolla, CA) had been added. After trituration with a wide-bored pipette, 2 ml of the supernatant fluid with isolated cells were transferred to the recording chamber. The cells were allowed to settle down for about 30 min, after which they were continuously superfused with GMR throughout the experiment, which typically lasted for about 3–5 hr. ORNs were visually identified by their characteristic morphology and distinctive features including a spherical or ovoid soma (5–8 μm diameter) and a single dendrite (~3 μm in diameter) arising from the soma, which terminated in a swelling (~2–3 μm in diameter), the dendritic knob, from which a number of fine cilia extend in vivo. The dissection and the experiments were performed at room temperature (20–22°C).

Solutions and Perfusion System

A special multi-barrel perfusion system was set up to enable us to change solutions very effectively and rapidly across the patch of membrane (*see* Fig. 2). The system consists of a sylgard chamber glued onto a standard microscope slide, which was divided into 2 compartments connected by a narrow canal. One compartment served to store the cells during the experiment, and in it cells were continuously superfused by General Mammalian Ringer, containing (in mM): NaCl 140, KCl 5, $CaCl_2$ 2, $MgCl_2$ 1, glucose 10, 4-(2-hydroxy-ethyl)-1-piperazineethanesulfonic acid (HEPES) 10 (titrated to pH 7.4 with KOH). On-cell patches were obtained among the cilia on the dendritic knobs or from the soma of olfactory receptor neurons, and excised in inside-out patch configurations by a brief air exposure. The other compartment was equipped with perfusion outlets allowing exposure of excised patches to different test solutions. After the formation and excision of patches, the pipette with membrane patch was transferred through the inter-compartmental canal and visually positioned in front of the outflow of the perfusion tube array through which the control and various test solutions flowed.

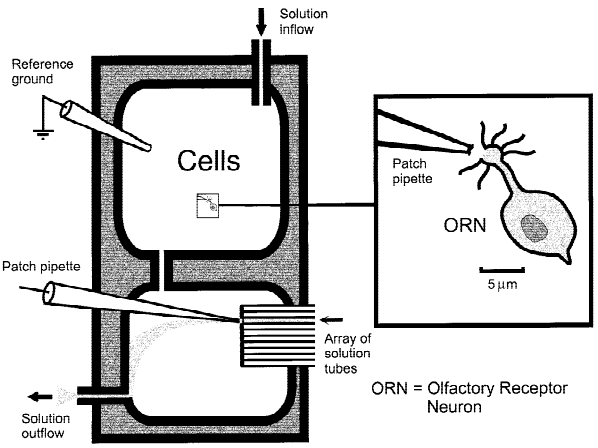

Fig. 2. The special multi-jet perfusion system used in our experiments and used for changing solutions across the patch of membrane spanning the tip of the patch-pipette. As already described in Methods, the system consists of 2 compartments connected by a narrow canal. The compartment, labelled as "Cells", served to store dissociated olfactory receptor neurons during the experiments, with the cells being continuously superfused by General Mammalian Ringer's solution (GMR). On-cell patches were formed in this compartment. The figure in the inset (on the right) shows how the membrane patches were obtained. The patch-pipette was positioned against the knob membrane amidst the cilia (not visible) and an inside-out patch was excised from it. The second compartment was equipped with an array of perfusion tubes through which different solutions flowed. These bathed the patch of membrane spanning the tip of the patch pipette, visually positioned in front of the outflow of one of the perfusion tubes. Solutions were changed rapidly and effectively by moving the perfusion tubes with the microscope stage on which the whole system was mounted.

For the study of single cAMP-gated channels, the ionic composition of the solution filling the patch pipette and the extracellular solution contained (in mM): NaCl 145, NaOH 5, HEPES 10, EGTA 11 (pH 7.4).

For the study of single IP_3-gated channels, the ionic composition of the solution filling the patch pipette and extracellular solution contained (in mM): NaCl 140, KCl 5, $CaCl_2$ 2, $MgCl_2$ 1, glucose 10, HEPES 10 (pH 7.4).

For the study of macroscopic cAMP and IP_3-gated currents, a symmetrical ionic solution with composition (in mM): NaCl 140, KCl 5, $CaCl_2$ 2, glucose 10, HEPES 10 (pH 7.4) was used for the IP_3 currents. However, for the cAMP currents the cytoplasmic side had a divalent ion free solution with composition the same as that used in the single-channel study of cAMP-gated channels, since intracellular Ca^{2+}

could significantly reduce the affinity of the channels for cAMP (Frings et al., 1995; Balasubramanian et al., 1996).

Electrophysiological Recordings

The recording setup consisted of an inverted microscope (Olympus IX70) placed in a Faraday cage. Electrodes were pulled from thick-walled borosilicate glass tubing (GC15 OF-15, Clark Electromedical Instruments, Reading, UK) and fire-polished to a final resistance of 8–18 MΩ when filled with pipette solution. The pipettes were also coated with Sylgard (Dow Corning, Midland, MI). The single channels and macroscopic currents were studied in excised inside-out patches from membranes of the dendritic knobs and soma of isolated olfactory receptor neurons using standard patch-clamp techniques (Hamill et al., 1981). For measuring macroscopic cAMP and IP_3 current responses, step-voltage pulses between −60 to +60 mV, from a holding potential of 0 mV, were applied both in the presence and absence of cAMP or IP_3. The cAMP- and IP_3-activated currents were obtained from the difference between recordings in the presence and absence of each agonist. In all the experiments, the currents and potentials are represented with the usual sign convention: currents flowing from the intracellular side of the membrane patch (bath solution) to the extracellular side (pipette solution) are positive and are plotted upwards and membrane potentials are given as the potential of the internal (cytoplasmic) solution with respect to the external one. Liquid junction potentials were calculated for each solution, using the Windows version of the software program JPCalc (Barry, 1994) and the appropriate corrections were applied to the membrane potential values. Currents were measured using an Axopatch 1D amplifier (Axon Instruments, Foster City, CA). The current signals were filtered at 2 kHz with the 4-pole bessel filter of the amplifier and digitized at 10 kHz via a DigiData 1200 interface (Axon Instruments), monitored online and stored in an IBM-compatible computer running pCLAMP 8 software (Axon Instruments, Foster City, CA). This software was also used to control the D/A converter for generation of voltage-clamp protocols and to analyze the generated data.

Single-channel conductances were measured both directly and by fitting Gaussian distributions to amplitude histograms (bin widths varied from 0.05 to 2 pA), before kinetic analysis. All single-channel analyses used the pClamp 8 software. Only events longer than three times the rise time of the filter (cutoff ~ 0.16 msec) were accepted for further kinetic analysis. Open- and closed-time distributions were constructed from event lists generated with a 50% threshold criterion, binned logarithmically with seven or eight bins per decade, and plotted against the square root of their frequency. Time constants describing the distribution of binned closed and open times were obtained by fitting Gaussian functions to these distributions with a least-squares optimization procedure.

All data are expressed as the mean ± SEM, with the number of observations, *n*, in parentheses.

Results

The Presence of IP_3-Gated and CNG Channels in the Dendritic Knob and Soma of Rat ORNs

In the absence of either IP_3 or cAMP in the bath and under symmetrical control conditions, no single-channel activity was seen. The addition of IP_3 (2–10 μM) or cAMP (2–20 μM in divalent cation-free solution) to the solution superfusing the cytoplasmic side of the patch, elicited clear single-channel currents and also bursts of channel currents in membrane patches from both the dendritic knob and soma of rat ORNs. Cyclic AMP-activated currents were more frequently observed than IP_3-activated currents for both dendritic knob and soma patches. In the dendritic knob, 83% of the patches (25 out of 30) responded to cAMP, whereas for the same patches, only 36% (11 out of 30) responded to IP_3. Similarly in the soma, 38% patches (15 out of 40) responded to cAMP, whereas for the same patches, only 15% (6 out of 40) responded to IP_3.

Characterization of IP_3-Gated Single Channels in the Dendritic Knob

Figure 3*A* displays outward current fluctuations with some clear single-channel openings in response to the addition of 2 μM IP_3 to the cytoplasmic side of an inside-out patch from the dendritic knob at a membrane potential of +40 mV. These IP_3-activated currents could be classified further into two groups (large or small conductances) on the basis of their single-channel conductance (Fig. 3a; expanded scale). Figure 3*B* is an amplitude histogram of a trace showing both large and small IP_3-activated channels. The histogram depicts three current peaks: one at "0" pA, relating to the closed state, and the other two at 0.52 and 1.37 pA, respectively. The average conductances of the small and large channels were 14 ± 3 pS ($n = 4$) and 40 ± 7 pS ($n = 9$), respectively. In addition, direct measurements of single-channel amplitude gave values similar to those obtained from the amplitude histogram. In general, both conductance types were observed in the same patch.

Large-Conductance IP_3-Gated Channels

The average conductance of the large IP_3-gated channel was 40 ± 7 pS (n = 9). Figure 4*A* shows a recording from a dendritic knob patch containing essentially only large conductance channels at a membrane potential of +40 mV. This channel, which displayed both single-openings and bursts, was comprised of a series of openings separated by brief closures. When the membrane potential of the patch was changed to −40 mV, clear single channel openings were still seen, and the burst behavior seemed to be unaltered. Figure 4*B* shows the corresponding amplitude histogram, the peak corresponding to an open-channel amplitude of 1.46 pA (37 pS; $n = 5$). The current-voltage relationship (Fig. 4*C*), obtained by plotting mean current amplitude ($n = 4$) versus membrane potential, was almost linear and reversed near 0 mV under symmetrical ion concentration conditions. In order to describe the channel kinetics, dwell-time histograms were constructed (Fig. 4*D* & *E*).

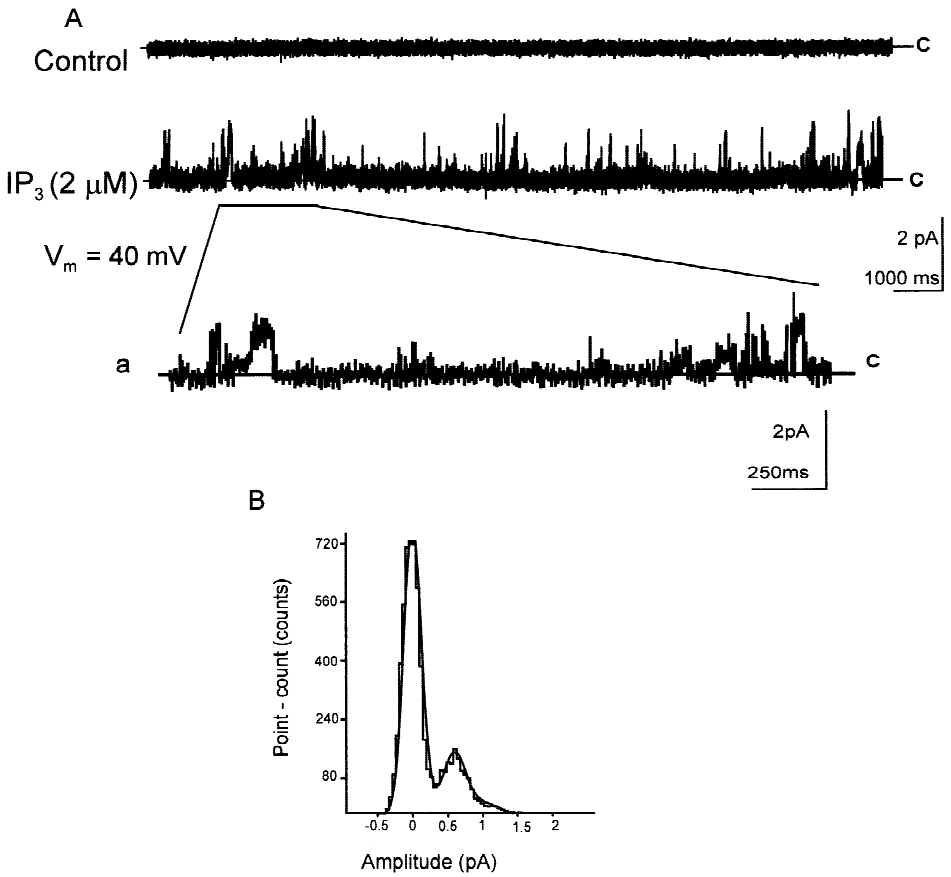

Fig. 3. IP_3-Evoked unitary currents in inside-out membrane patches from the dendritic knobs of rat olfactory receptor neurons. (*A*) Basal currents prior to control and after IP_3 perfusion of 2 μM IP_3 on the internal face of a patch. Most of the channel openings were not resolved due to the compressed timescale. Membrane Potential = +40 mV. Expanded timescale (*a*) shows clear channel openings, "*c*" denotes closed-state. (*B*) Amplitude histogram from the membrane patch in *A*, fit by Gaussian distributions with mean peak values of 0.52 and 1.37 pA respectively. The first peak ("0" pA) corresponds to the closed-state of the channel.

Both the open- and closed-states were significantly better fitted with the sum of three exponentials having open time-constants of 0.8 ± 0.2, 5.2 ± 1.1 and 108 ± 40 msec ($n = 3$), whereas the closed time-constants were 0.7 ± 0.4, 2.9 ± 1.3, 23.2 ± 17.6 msec ($n = 3$). The mean open time-constant of the channel was 32 ± 17 msec ($n = 5$), whereas the mean closed time-constant was 8.1 ± 6.8 msec ($n = 5$). The mean open- and closed-times and conductance of the large IP_3-gated channel are given in Table 1.

Small-Conductance IP_3-Gated Channels

The average IP_3-gated small-conductance channel was 14 ± 3 pS ($n = 4$). Figure 5*A* shows a record of IP_3-induced current fluctuations occurring in a patch taken from a dendritic knob membrane containing a small-conductance channel at a membrane potential of −35 mV. The channel openings were small and brief and seemed more flickery than the large-conductance channel. The corresponding amplitude histogram (Fig. 5*B*) was, however, fitted significantly better with two Gaussian functions than with just one. The small, not very distinct open peak corresponds to an amplitude of −0.51 pA (14.5 pS). The mean current amplitude versus voltage relationship for this small-conductance channel (Fig. 5*C*) was essentially linear, with a reversal potential close to zero under our symmetrical ion concentration conditions. The open-state (Fig. 5*D*) was fitted with two exponentials with time constants of 1.0 ± 0.5 and 4.5 ± 1.2 msec ($n = 3$), while the closed-state (Fig. 5*E*) required a three-exponential fit, with time constants of 0.9 ± 0.4, 12.3 ± 6.9 and 120 ± 43 msec ($n = 3$). The mean open-time for the small conductance channel was 1.84 ± 0.54 msec ($n = 3$) and the mean closed-time was 25.7 ± 15.4 msec ($n = 3$). The mean open- and closed-times and conductance of the small IP_3-gated channel are given in Table 1. A comparison of the mean open-times between small and large IP_3-gated channels in the dendritic knob showed that the small-conductance IP_3-gated channel

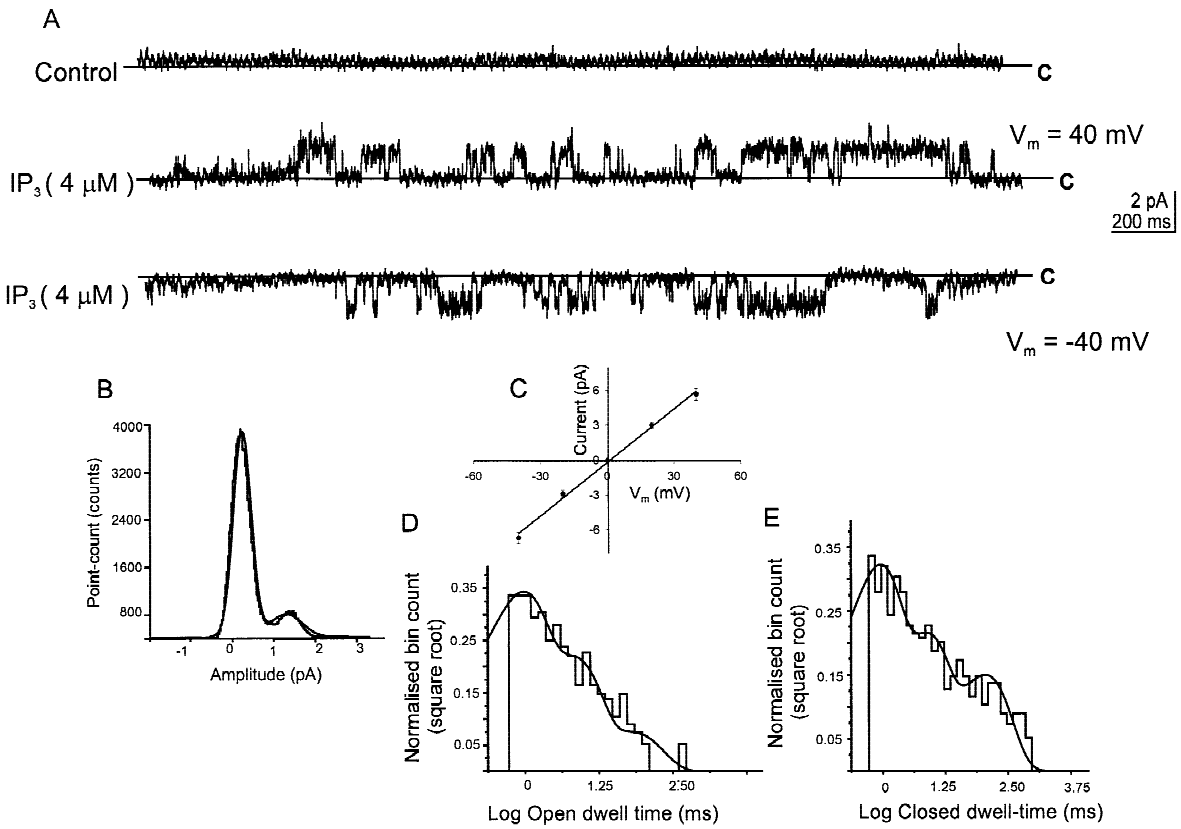

Fig. 4. Large conductance (40 ± 7 pS) IP_3-evoked, unitary currents across inside-out patches of membrane from the dendritic knob of a rat olfactory receptor neuron. (*A*) Basal currents prior to (*control*) and after (*IP*$_3$) perfusion of 4 μM IP_3 on the internal face of a patch. V_m is the membrane potential and "*c*" denotes the closed-state. (*B*) Amplitude histogram from the membrane patch in *A*, fit by a Gaussian distribution with mean peak value of 1.46 pA. The peak ("0" pA) corresponds to the baseline. (*C*) Plot of the macroscopic mean current-voltage relationship in symmetrical solutions ($n = 4$). Voltage is in mV on the abscissa and current in pA on the ordinate. (*D*) Open-time histogram distribution of the above IP_3-gated channel. The histogram had a three-exponential fit. (*E*) Closed-time histogram distribution of the IP_3-gated channel also had a three-exponential fit.

Table 1. Single-channel conductance and kinetic parameters of IP_3-gated channels in the dendritic knob of ORNs.

Small–Conductance Channel 14 ± 3 pS ($n = 4$)		Large–Conductance Channel 40 ± 7 pS ($n = 5$)	
Mean open-time (msec)	Mean closed-time (msec)	Mean open-time (msec)	Mean closed-time (msec)
1.8 ± 0.5	26 ± 15	32 ± 17	8.1 ± 6.8

Values are the mean ± SEM.

had a shorter open-time (1.8 ± 0.5 msec; $n = 3$) than the large-conductance channel (32 ± 17 msec; $n = 5$). Similarly, the mean closed-time of the smaller channel (26 ± 15 msec; $n = 3$) was greater than that of the large channel (8.1 ± 6.8 msec; $n = 3$).

Inhibition by Ruthenium Red

Figure 5*A* also illustrates the effect of ruthenium red on the IP_3-gated channels in an inside-out patch from the dendritic knob of an ORN. Consistent with the known effects of ruthenium red on olfactory IP_3-gated non-specific cation channels (Restrepo et al., 1990, 1992; Fadool & Ache, 1992; Suzuki, 1994; Honda et al., 1995; Lischka et al., 1999), 10–20 μM ruthenium red abolished the channel activity. Ruthenium red (10–20 μM) also blocked the large-conductance channel (*data not shown*).

Characterization of IP_3-Activated Single-Channels in Soma Patches

The percentage of inside-out patches from the soma membrane responding to IP_3 was very low (15%) and it was very difficult to get single-channel IP_3 records. Figure 6*A* shows a trace with IP_3-gated channels from an inside-out membrane patch of soma, depicting both large- and small-conductance channels. Both channel types are more clearly seen in the expanded section of the trace (Fig. 6*a*). The corresponding amplitude histogram (Fig. 6*B*) was fitted with three Gaussian functions with

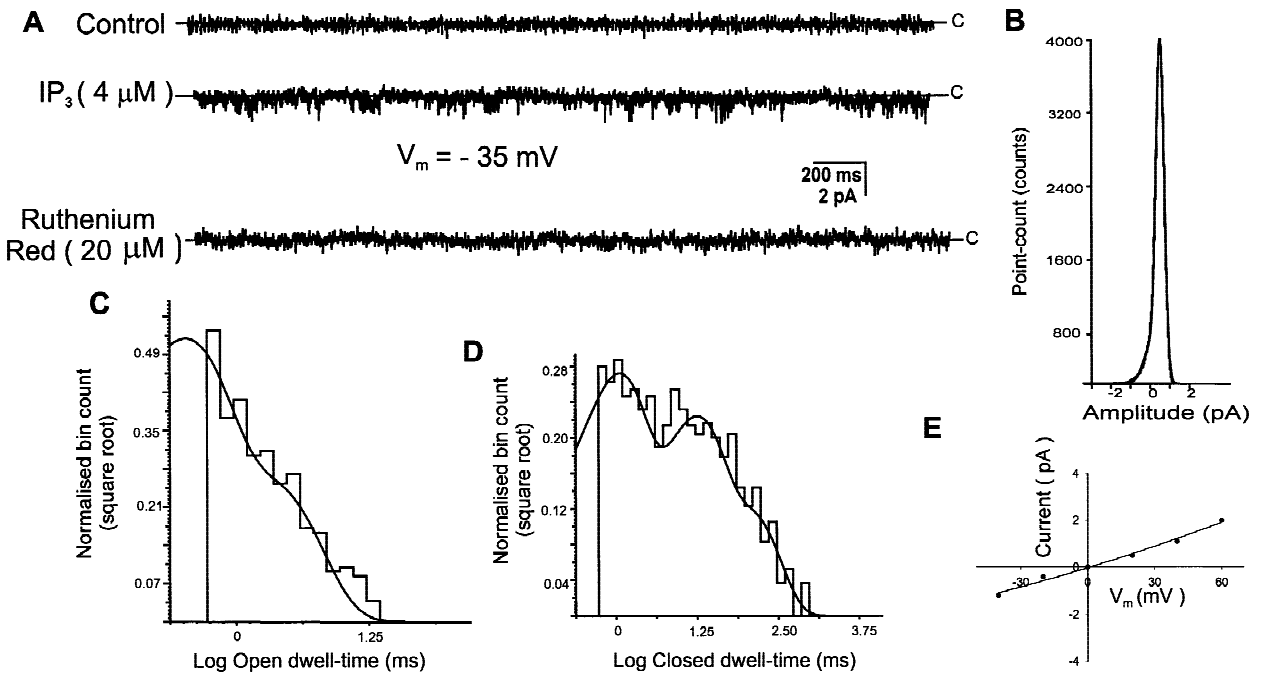

Fig. 5. Small-conductance (14 ± 3 pS) IP_3-evoked, unitary currents across inside-out patches of membrane from the dendritic knob of a rat olfactory receptor neuron. (*A*) Basal currents prior to (*control*) and after IP_3 perfusion of 4 μM IP_3 on the internal face of a patch. Membrane potential, V_m, = −35 mV. The effect of 20 μM Ruthenium Red (bottom trace) was to inhibit the IP_3-gated channel in the membrane patch. "*c*" denotes the closed-state. (*B*) Amplitude histogram from the membrane patch in (*A*), fit by Gaussian distribution with a mean value of −0.51 pA. The peak ("0" pA) corresponds to the baseline. (*C*) The open-time histogram distribution of the IP_3-gated channel shows a two-exponential fit. (*D*) The closed-time histogram distribution of the IP_3-gated channel shows a three-exponential fit. (*E*) Plot of the macroscopic mean current-voltage relationship for the above membrane patch in symmetrical solutions.

single-channel amplitudes corresponding to 0.53 and 1.58 pA and giving similar conductances (13 and 40 pS) to those found in knob patches.

An Analysis of Single CNG Channels in Dendritic Knob Patches

Single-channel activity activated by cAMP was studied in divalent cation-free internal solution. Figure 7*A* shows a trace recording of cAMP-induced current in a patch from the dendritic knob of an ORN at a membrane potential of −40 mV. The control trace showed no channel openings in the absence of cAMP. With the addition of 15–20 μM cAMP to the solution bathing the cytoplasmic side of the membrane patch, channel activity can be readily seen. In this trace, discrete single-channel openings are not discernible. However, more than one conductance state, together with multiple-openings, were present. The high channel activity with flickery behavior and multiple openings is also seen in the expanded trace (Fig. 7*a*). This activity is probably due to the gating of many cAMP-gated channels contained in the patch. Plotting this single-channel activity as an amplitude-histogram (Fig. 7*B*) indicates that there are three conductance states, which were consequently fitted with at least three Gaussians. The first peak corresponds to the closed-state, whereas the other peaks are fused with single-channel current amplitudes ranging from −1.3 to −2.5 pA to give conductances of 32–63 pS. In addition, the tail of the amplitude histogram extends up to −3.5 to −4 pA with conductances of 87–100 pS. Under our experimental conditions, the mean open- and closed-times of the channel were 2.7 ± 0.5 msec and 19.7 ± 12.8 msec (n = 5) respectively.

An Analysis of Single CNG Channels in Soma Patches

Figure 8*A* shows a record of cAMP-induced currents in a patch from the soma of an ORN at a membrane potential of −40 mV. The control trace in divalent cation-free solution showed no channel openings (*not shown*). The addition of 50–60 μM cAMP to the solution bathing the cytoplasmic side of the membrane patch showed clear channel activity. The trace depicts flickery behavior of the channel with bursts of channel activity and single-channel openings. The single-channel openings are more clearly seen in the expanded section of the trace

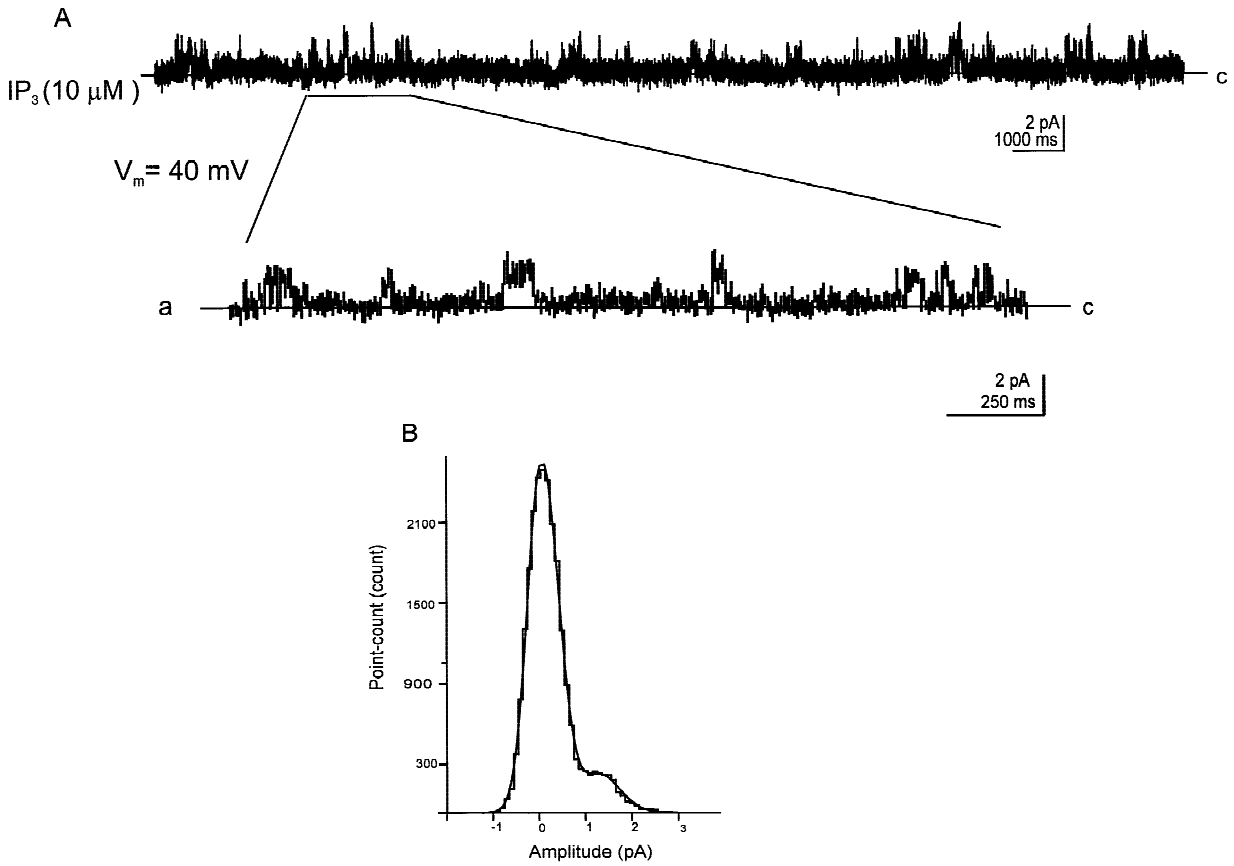

Fig. 6. IP_3-evoked unitary currents across inside-out patches of membrane from soma of rat olfactory receptor neurons. (*A*) Single-channel currents after perfusion of 10 μM IP_3 on the internal face of a patch, with $V_m = 40$ mV. Most of the channel openings are not resolved due to the compressed time-scale. Expanded time-scale (*a*) shows clear channel openings. "*c*" denotes closed-state. (*B*) Amplitude histogram for the membrane patch in (*A*), fit by Gaussian distributions with mean peak values of 0.53 and 1.52 pA respectively, the first peak corresponding to closed-state of the channel.

(Fig. 8*a*). The accompanying amplitude histogram (Fig. 8*B*) illustrates two identifiable peaks fitted with two Gaussians. The first peak at "0" pA corresponds to the closed-state, whereas the second clear peak (−1.42 pA) represents the single-channel current amplitude and an average single-channel conductance of 35 ± 3 pS ($n = 6$). Under our experimental conditions, the mean open-time of the channel was 1.9 ± 0.4 msec and the mean closed-time 39 ± 30 msec ($n = 3$).

The Relative Densities of CNG and IP_3-Activated Channels in Soma and Dendritic Knob Membranes

To determine the relative contribution of the two second messengers (cAMP and IP_3) in olfactory transduction, we measured the relative density of CNG and IP_3-gated channels in inside-out patches from both the dendritic knob and soma in rat ORNs. In each case, the pipette (extracellular) solution contained 2 mM [Ca^{2+}], although the cAMP cytoplasmic solution did not contain any Ca^{2+}. Inside-out excised membrane patches from the dendritic knob of ORNs were exposed to 0.1, 2, 10 and 100 μM cAMP and IP_3 was applied (separately) to the cytoplasmic side. Macroscopic current traces were recorded in response to voltage steps, with control currents in the absence of agonists being subtracted. Figure 9 (*A* & *B*) shows examples of current traces recorded when 100 and 10 μM cAMP and IP_3 were applied to an inside-out patch from the dendritic knob, while Fig. 9*C* shows the averaged current-voltage relationship ($n = 3$) for a dendritic knob patch after an application of 100 μM cAMP and IP_3. Both I-V plots showed linearity without any rectification, with a zero reversal potential. However, the magnitude of the current amplitude was much greater with cAMP than with IP_3. A preliminary dose-response curve is shown for IP_3 in Fig. 9*D* for dendritic knob patches, in which the current amplitudes at 100 μM IP_3 were normalized to 1 ($V_m = -60$ mV, $n = 3$). The data were fitted by a curve using a Hill-type equation:

$$I_{norm} = C^h/[C^h + EC_{50}{}^h] \quad (1)$$

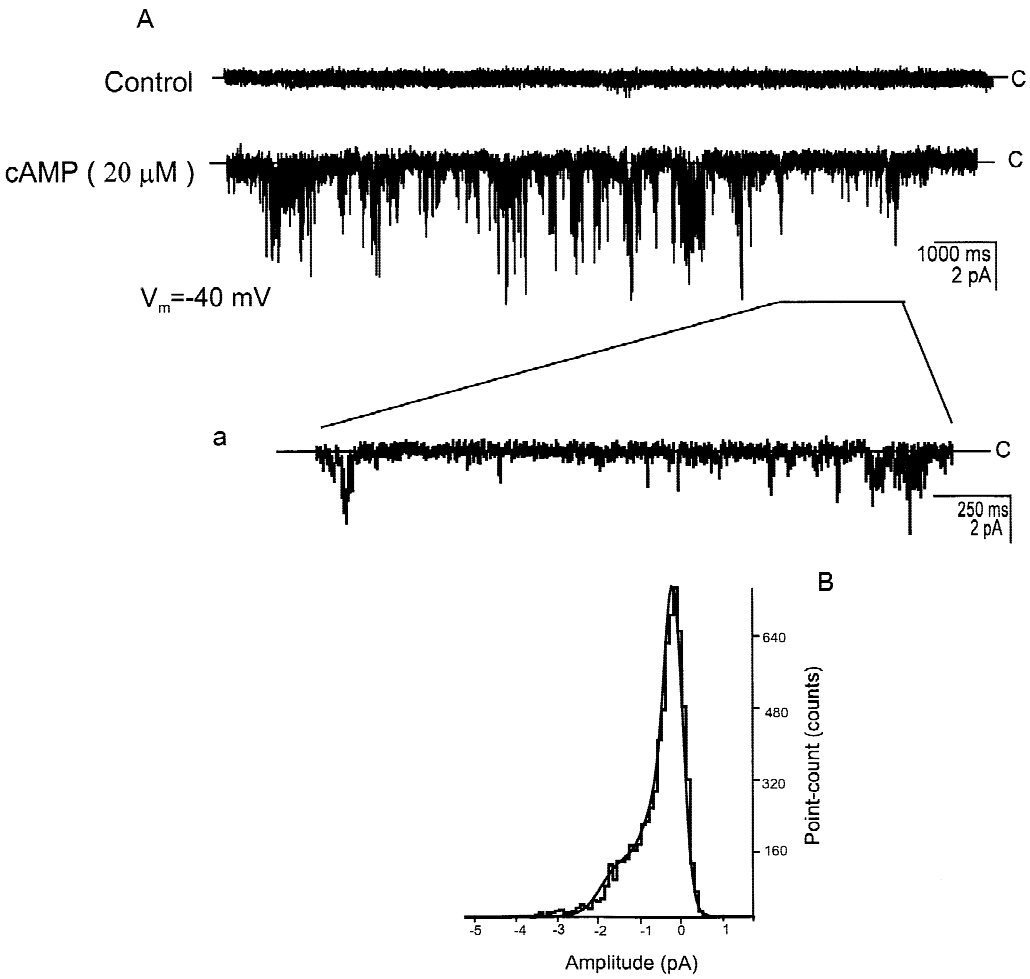

Fig. 7. Cyclic AMP-evoked unitary currents across inside-out patches of membrane from the dendritic knob of rat olfactory receptor neurons. (*A*) Basal currents prior to (control) and after perfusion of 20 μM cAMP on the internal face of a patch. Clear single-channel openings are not readily resolved due to the compressed time-scale. Due to the amount of channel activity, even the expanded time-scale does not show clear single-channels. "*c*" denotes closed-state. (*B*) Amplitude histogram from the membrane patch in (*A*), fit by gaussian distributions with mean peak values of −1.3 and −2.5 pA. Also, the tail of the amplitude histogram extends up to −3.5 to −4 pA. The first peak ("0" pA) corresponds to the closed-state of the channel.

Where I_{norm} is the normalized current, C is the IP_3 concentration and h is the Hill coefficient. Fitting averaged results for IP_3 for 3 cells revealed an EC_{50} of 36 μM and a Hill coefficient of 1.1, compared to an EC_{50} of 3 μM with cAMP reported previously in our lab (with zero pipette $[Ca^{2+}]$; Balasubramanian et al., 1996). Figure 10*A* is an example of the current traces recorded when 100 μM cAMP and IP_3 were applied to an inside-out patch from the soma membrane. Figure 10*B* shows the I-V relationship for averaged data ($n = 4$) with 100 μM cAMP and IP_3 for such patches. In this case, both the current amplitudes were much smaller than they were in the dendritic knob patches and again the IP_3-activated current was much smaller than the cAMP-activated one.

The relative densities of CNG and IP_3-gated channels in the inside-out patches from the soma and dendritic knob membranes of ORNs were calculated by two different methods. The first method involved the initial calculation of the total number, N, of CNG and IP_3-gated channels and the unitary current amplitude, i, for the patch. The values were determined from the following equation (Hille, 1984) relating variance (σ^2) and mean current amplitude (I):

$$\sigma^2/I = i - I/N \tag{2}$$

This equation indicates that plotting σ^2/I against I gives a straight line with a slope of $-1/N$ that crosses the ordinate at the unitary current amplitude, i. The variance (σ^2) in this equation was calculated from the difference in variance obtained in the presence and absence of agonist. The mean agonist-induced current, I, was obtained in the presence of 2, 10 and 100 μM cAMP or IP_3. Only patches that had both cAMP- and IP_3-gated channels

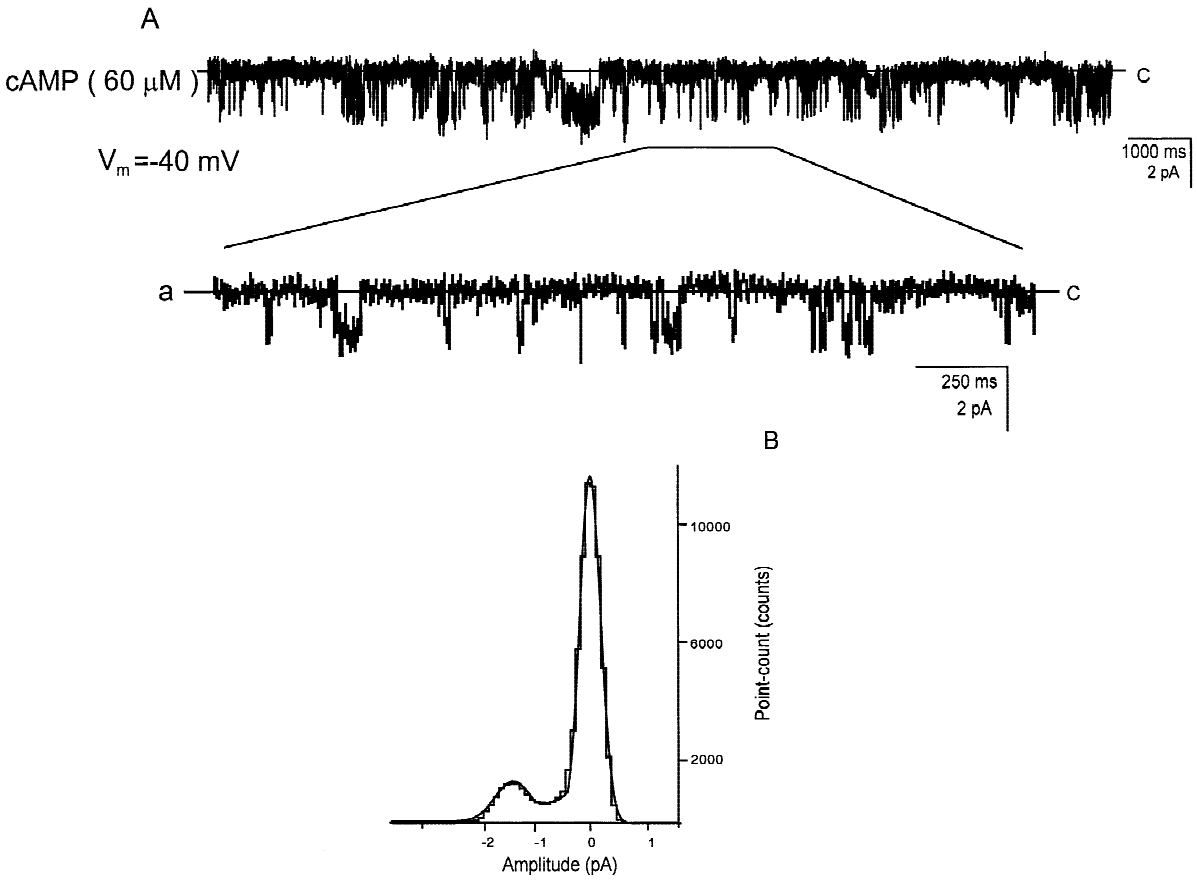

Fig. 8. Cyclic AMP-evoked unitary currents across inside-out patches of membrane from the soma of rat olfactory receptor neurons. (*A*) Single-channel currents after perfusion of 60 μM cAMP on the internal face of a membrane patch, with $V_m = -40$ mV. Clear single-channel openings are not resolved due to the compressed time-scale. The expanded time-scale (*a*) does show distinct single-channel openings. "*c*" denotes closed-state. (*B*) Amplitude histogram from the membrane patch in *A*, fit by Gaussian distribution with mean peak value of −1.42 pA. The first peak ("0" pA) corresponds to the closed-state of the channel.

were used for these measurements. For each patch, σ^2/I was plotted against I for that patch and the value of N determined. These values were averaged and the SEM determined for the whole set of patches. The average value of σ^2/I was also plotted against I for each channel and the results are shown in Fig. 11. This method gave an average number of CNG channels in dendritic knob patches of 333 ± 19 ($n = 6$) channels. This, in turn, gave an estimate of average CNG channel density of ~1000 μm^{-2} (the membrane patch was assumed to be circular with an average patch tip diameter of ~0.65 μm; based on an estimate of the pipette tip diameter of ~0.6–0.7 μm and pipette resistance of ~12–15 MΩ). Similar measurements for the same set of patches gave a mean number of IP_3-gated channels in an excised patch of 29 ± 5 ($n = 6$), with an estimated channel density of ~85 μm^2.

For the second method, mainly used to confirm the results of the first method and done on the same patches as the first method, the following equation was used:

$$I = i \cdot N \cdot P_o \tag{3}$$

where N is the number of channels that can be activated in a patch, i is the unitary current [obtained using Eq. (2)], P_o is the open probability of the channel and I is the total current. If the assumption can be made that $P_o = 1$, then N simply $= I/i$. In general, the value of N then gives the minimum number of channels that can be activated in a patch, since $P_o < 1$ would imply a larger value of N. Balasubramanian et al. (1995) and Restrepo (1992) reported that 100 μM of cAMP and 30 μM IP_3, respectively, were saturating doses and gave maximal responses and presumably $P_o \approx 1$. This was certainly valid for cAMP (Fig. 7 of Bönigk et al., 1999, for their experiments on rat ORNs, where $P_o = 1.0$ above about 30 μM). It should also be noted that the examples of current records given in this paper (e.g., Fig. 8) were especially chosen to show clear single channel transitions and therefore were likely to have had a lower open

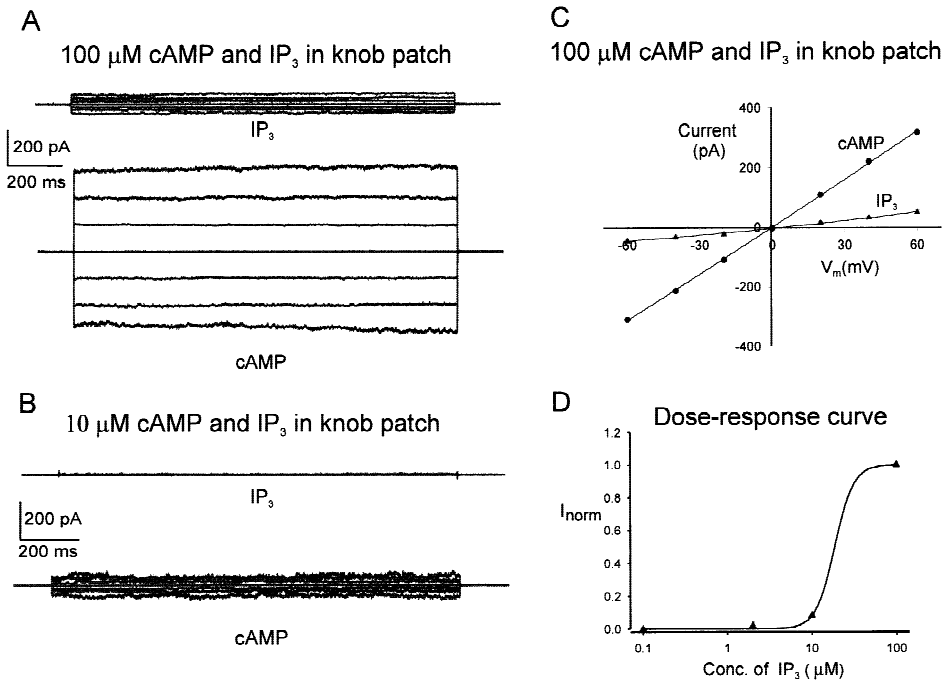

Fig. 9. Cyclic AMP- and IP_3-evoked currents across membrane patches from the dendritic knob of rat olfactory receptor neurons. (*A*) Currents activated by 100 μM cAMP and IP_3. Voltage pulses of 1.6 sec duration, from −60 (bottom trace) to +60 mV (top trace) in 20 mV steps, were generated from a holding potential of 0 mV. Each trace was obtained as the difference between the currents measured in the presence and absence of cAMP and IP_3 in the perfusion solution. (*B*) Currents activated by 10 μM cAMP and IP_3. Voltage pulses of 1.6 sec duration, from −60 to +60 mV in 20 mV steps, were generated from a holding potential of 0 mV. Each trace was obtained as the difference between the currents measured in the presence and absence of cAMP and IP_3 in the solution. (*C*) Averaged current-voltage relationship of CNG and IP_3 channels activated by 100 μM cAMP and IP_3 for the same patches ($n = 3$). (*D*) A preliminary IP_3 dose-response relationship. Data points are averaged values of current at −60 mV, normalized (I_{norm}) to the maximum current obtained in the presence of 100 μM IP_3 ($n = 3$). The curve was fitted by a Hill type equation, using an EC_{50} of 36 μM for IP_3 (Hill coefficient, $h, = 1.1$).

probability than most of the other patches. Using this second method for the response to 100 μM of agonist, the value of N for cAMP-gated channels in the dendritic knob gave a rough estimate of ~300, implying a channel density of ~900 μm^{-2}. Hence, the density of CNG channels estimated by each of the two different methods was similar. Balasubramanian et al. (1995) also reported similar numbers of CNG channels in membrane patches from dendritic knobs. Using the second method, the value of N for the IP_3-gated channels was calculated as ~25, to give a channel density of ~75 μm^{-2}. Indeed, even if the maximum P_o of IP_3-gated channels was only ~0.7, it is still clear that the CNG channel density would be an order of magnitude greater than that of the IP_3-gated ones.

Comparable calculations indicated that the numbers of CNG and IP_3-gated channels were much less in patches from the soma than from the knob. In the soma, the mean number of channels in the excised patch in response to cAMP was calculated to be 45 ± 3 ($n = 7$), to give a channel density of ~57 μm^{-2} (the patch membrane was assumed to be circular, with tip diameter ≈1 μM and pipette resistance ≈6–10 MΩ). In contrast, the number of IP_3-gated channels in a soma patch was 10 ± 2, to give an IP_3-gated channel density of only ~13 μm^{-2}. Once again, the CNG and IP_3-gated channel densities obtained by the second method were somewhat similar to those obtained using the first method.

Hence, there was a much smaller density of IP_3-gated channels compared to CNG channels in both the knob and the soma. There was also a much lower density of both CNG and IP_3-gated channels on the soma than on the knob. These data, together with the fractions of patches responding to either cAMP or IP_3, are summarised in Table 2.

Discussion

We have now further confirmed the presence of IP_3-gated channels in rat ORNs and shown that both IP_3-gated and CNG channels can co-exist in ORN membrane patches. Using inside-out patches from fresh acutely-dissociated rat ORNs, we found two types of IP_3-gated

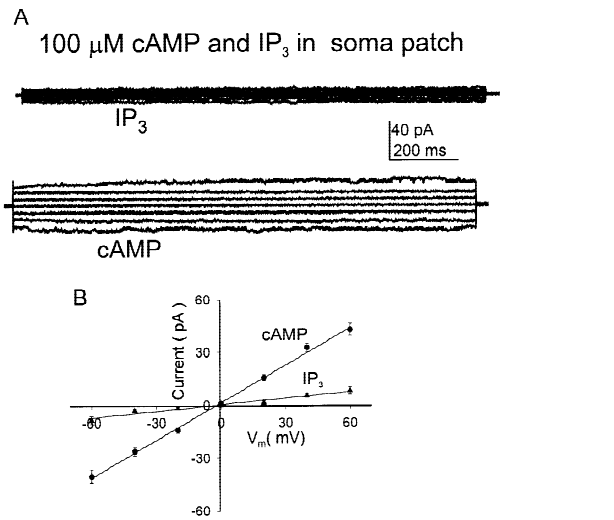

Fig. 10. Cyclic AMP- and IP_3-evoked currents across membrane patches from the soma of olfactory receptor neurons. (*A*) Currents activated by 100 μM cAMP and IP_3. Voltage pulses of 2 sec duration, from −60 to +60 mV in 20 mV steps, were generated from a holding potential of 0 mV. Each trace was obtained as the difference between the currents measured in the presence and absence of cAMP and IP_3 in the perfusion solution. (*B*) Averaged current-voltage relations of CNG and IP_3-gated channels, activated by 100 μM cAMP and IP_3 for the same patches ($n = 4$). Note that the scales are very different from those used for the dendritic knob patches in Fig. 9.

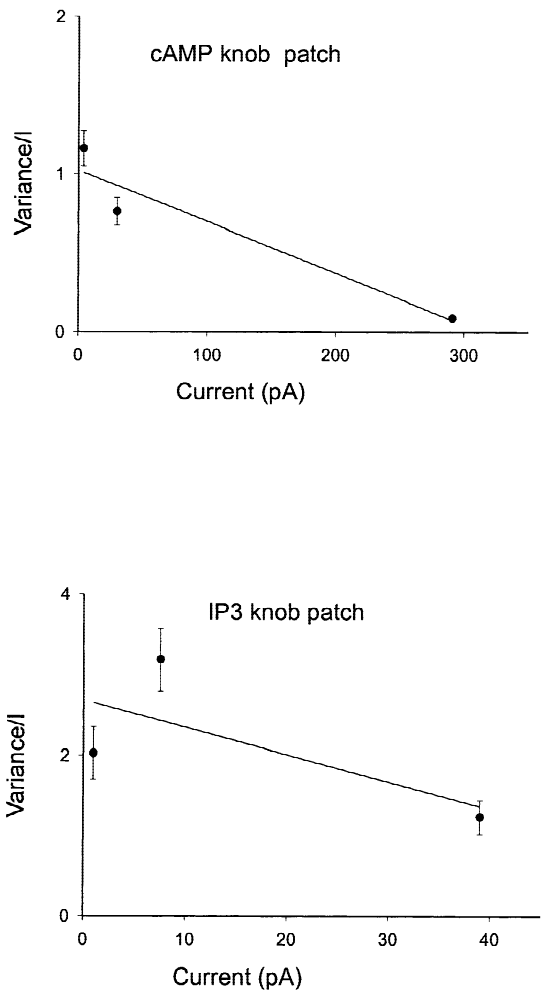

Fig. 11. The relationship between variance/*I* and *I* for the current response induced by cAMP and IP_3, for the same set of dendritic knob patches. Data were obtained by applying cAMP and IP_3 at various doses to the cytoplasmic side of a patch membrane excised from dendritic knob, and errors are SEM. (*A*) Relationship between variance/*I* and *I* for the membrane patch from the dendritic knob induced by cAMP (*A*) and that induced by IP_3 (*B*). It should be noted that the value of *N*, the number of channels per patch, and its SEM in the text, were determined by averaging the values determined from similar individual plots for each patch.

channels in the dendritic knob and soma membranes. We have also shown that although both cAMP and IP_3 can directly gate the activated channels and elicit unitary membrane currents, the relative density of IP_3 channels is very much less than that of CNG ones in both membranes, and the density of both is very much higher in the dendritic knob.

It is of interest to note that Noé and Breer (1998), using very different techniques, namely those of Ca^{2+} imaging and single-cell RT-PCR, have also demonstrated that both second messenger systems can coexist in a sub-population of olfactory sensory neurons, in support of the concept of dual transduction in olfaction.

Second Messenger cAMP- and IP_3-Gated Conductances

A single-channel analysis of CNG and IP_3-gated channel properties of the ORNs (dendritic knob and soma) showed that characteristic features distinguished these two second-messenger-activated ion channels from each other. The high activity of CNG channels in the dendritic knob patches suggested the presence of more than one cAMP channel in each patch, as previously observed by others (Hatt & Ache, 1994). For the IP_3-gated channels, two channel types with different conductances were also observed in the dendritic knob patches: one large (40 ± 7 pS) and one small (14 ± 3 pS). IP_3-gated channels with similar conductance properties were also observed in soma membrane patches. The dwell-time (open and closed) histograms of the large-conductance IP_3-gated channel indicated that they have three kinetically distinguishable open and closed states. However, the dwell-time histograms of the small-conductance IP_3-gated channel suggested only two open states and three closed states. Whether these two IP_3-gated conductances represented two distinct types of IP_3 receptors or two different subconductance states of the same receptor, is not known.

Table 2. Relative densities of, and fraction of patches with channels responding to, CNG and IP_3-gated channels in membrane patches from the dendritic knob and soma of ORNs.

2^{nd} Messenger	Dendritic knob (Channels · μm^{-2})	Fraction of knob patches with channels	Soma (Channels · μm^{-2})	Fraction of soma patches with channels
CNG	1000	0.83	57	0.38
IP_3	85	0.36	13	0.15

Channel densities were calculated using the variance method (Eq. 2).

Fadool & Ache (1992) reported two IP_3-gated conductances (30 and 74 pS), which were similar in the dendrite and soma of cultured lobster ORNs. Both the small- and large-conductance IP_3-gated channels displayed channel bursts, but differed in their single-channel conductances and kinetics. Honda et al. (1995) observed in rat olfactory cilia membranes fused onto lipid bilayers, that ion channels opened by IP_3 could be classified into two groups (37 and 103–184 pS) that differed in terms of both conductance and kinetics. Hatt & Ache (1994) also reported two different IP_3-gated conductances (27 and 64 pS) in lobster dendritic membranes. As in our experiments, they observed briefer openings of the smaller conductance channel. Lischka et al. (1999) also observed two IP_3-gated conductances (64 ± 4 pS and 14 ± 1.7 pS) in the soma membrane of rat ORNs. IP_3-gated channels in some other cells display openings to multiple conductance levels (ER in cerebellum and SR in aortic smooth muscle; Ehrlich & Watras, 1988). Lischka et al. (1999) reported similar magnitudes of conductance levels for olfactory, cerebellar, ER and smooth muscle SR IP_3 receptors, suggesting that IP_3 receptor proteins in cerebellum and olfactory neurons may be identical.

Finally, we observed that ruthenium red (RR) decreased the amplitude of IP_3-induced current fluctuations from the rat olfactory dendritic knob and soma, as previously observed in lobster, catfish and rat (Restrepo et al., 1990; Fadool & Ache, 1992; Lischka et al., 1999). It should be noted that RR varies in its action on IP_3-activated channels in nonolfactory cells (e.g., it inhibits such channels in skeletal muscle SR but not in aortic smooth muscle; Ehrlich & Watras, 1988).

The Relative Densities and Contribution of cAMP and IP_3 Pathways in Olfactory Transduction

Following the observation of distinct CNG and IP_3-activated ion channels in the rat ORNs, we have now estimated the relative densities of CNG and IP_3-gated channels in both the soma and dendritic knob membranes. As far as the two channel types were concerned, in the dendritic knob membranes we observed a much higher density of CNG channels (~1000 μm^{-2}) than IP_3-gated channels (~85 μm^{-2}). With the fraction of patches at the knob responding to cAMP and IP_3 being 0.83 and 0.36 respectively, this gives an effective ratio of 27 for CNG/IP_3-gated channels at the knob. For the soma membrane, the channel density was much lower, being ~57 μm^{-2} and ~13 μm^{-2} for the CNG and IP_3-gated channels respectively. With the fraction of patches at the soma responding to cAMP and IP_3 being 0.38 and 0.15 respectively, this gives an effective ratio of 11 for CNG/IP_3-gated channels at the soma. For an order of magnitude calculation, a density of ~1000 cAMP-gated channels μm^{-2} on the dendritic knob membrane, a cylindrical dendritic knob of 2.5 μm diameter and 5 μm length, would imply a total of ~39,000 channels for the whole knob. For the IP_3-gated channels with a density of ~85 μm^{-2} on the dendritic knob membrane, a similar-sized knob would give an estimated total of ~3,300 channels. The precise value obviously depends very much on the size and shape of such knobs which vary considerably from one cell to another. However, what is clear here is that the relative density of CNG channels in the dendritic knob is at least an order of magnitude greater than that of IP_3-gated channels. Our findings on CNG channel density are in agreement with previous studies that reported a higher density in the dendritic knob membrane than in the soma membrane for rat ORNs (Kurahashi & Kaneko, 1991, 1993; Balasubramanian et al., 1995). Our estimates of the number of cAMP-gated channels in inside-out patches from the dendritic knob of rat olfactory receptor neurons are also in agreement with the data of Balasubramanian et al. (1995).

In amphibian ORNs, the highest density of CNG channels has been shown to be on the cilia, with estimates of channel density varying from about 450–7000 μm^{-2} (Nakamura & Gold, 1987; Kurahashi & Kaneko, 1991, 1993; Kleene et al., 1994), compared to values on the dendrite or cell body of about 2 μm^{-2} (Kurahashi and Kaneko, 1991). Although the values for the soma membranes of the rat ORN are very much larger than those of the amphibian, the CNG channel density value for the rat dendritic knob is tending towards the high values obtained for amphibian cilia. Unfortunately, we cannot directly investigate the properties of the cilia membrane in our preparation, but can merely use the dendritic knob values to approximate, and presumably underestimate,

the actual receptor density. On the basis of our data, it seems likely that the density of the CNG channels on the dendritic knob is at least an order of magnitude greater than that of the IP_3-gated channels. If the ratio increases with the absolute density of channels, as it does with the difference between soma and dendritic knob membranes, then the CNG to IP_3-gated channel ratio could be even greater in the cilia. However, two factors still need to be taken into account before any conclusions may be drawn about the relative contributions of the two second messenger pathways.

First, under physiological conditions, with the presence of a few mM Ca^{2+} in the extracellular fluid surrounding the cilia, the currents generated by the opening of each of the channels may be different. Even though olfactory CNG channels are very permeable to Ca^{2+} (e.g., bovine channels, $P_{Ca}/P_K \approx 5$; Frings et al., 1995), the channels are also blocked by Ca^{2+}, for which the channel has a high affinity. For example, in about 1 mM $[Ca^{2+}]_o$, the current drops to much less than 0.1 of its value in the absence of Ca^{2+} and about 50% of the current is carried by Ca^{2+} (Frings et al., 1995). These authors also showed that as $[Ca^{2+}]_o$ was increased up to about 3 mM, the current dropped even further and was almost exclusively carried by Ca^{2+}. It should be noted that the Ca-activated Cl^- channel is then able to amplify the depolarizing response to Ca^{2+} entering through these CNG channels. Measurements of IP_3-gated channels from olfactory cilia in bilayers have indicated that they have a lower calcium permeability with $P_{Ca}/P_K \approx 0.8$ (Restrepo 1992). However, a comparison of the averaged responses in the same patches responsive to saturating concentrations of both cAMP and IP_3 with equal extracellular (pipette) concentrations of $[Ca^{2+}]$ of 2 M can be seen in Figs. 9 and 10, where the magnitude of the macroscopic cAMP-induced current is almost an order of magnitude greater than that induced by IP_3 for membrane patches from both the dendritic knob and soma.

Second, the relative fraction of odorant receptors sensitive to cAMP and IP_3 on a particular ORN may be quite different and may depend heavily on the type of odorant, so that the proportion of cAMP- and IP_3-generated second messengers may be very different. It should also be noted that these currents do not have to be very large since olfactory ORNs possess a high membrane impedance (Firestein & Werblin, 1987), so that the cells are electronically compact and require only a few pA of injected current to elicit an action potential (Lynch & Barry, 1989; Kleene et al., 1994).

Nevertheless, in spite of some uncertainties relating to a precise evaluation of the relative contributions of the two second messenger pathways in response to odorant stimulation, we have demonstrated that CNG and IP_3-gated ion channels can occur in the same ORNs and the fact that the density of CNG channels is so much greater than the density of IP_3-gated ones, is, at the very least, consistent with the cAMP pathway being the predominant one.

Finally, one might ask what is the value of having two second messenger systems? In addition, to allowing for further options by having subsets of odorants that activate one or the other of the two signaling systems, it has been suggested by Vogl et al. (2000), that there can be cross-talk between the two pathways to fine-tune and modulate olfactory responses, with an increase in one second messenger tending to suppress the response of the other one.

We acknowledge the support of the Australian Research Council and the National Health and Medical Research Council of Australia. R.K. also acknowledges the support of a PhD Studentship from the CRC for International Food Manufacture and Packaging Science during the earlier part of this study. We also acknowledge helpful discussions with Dr. Graham A. Bell of the Centre for ChemoSensory Research at the University of New South Wales.

References

Balasubramanian, S., Lynch, J.W., Barry, P.H. 1995. The permeation of organic cations through cAMP-gated channels in mammalian olfactory receptor neurons. *J. Membrane Biol.* **146:**177–191

Balasubramanian, S., Lynch, J.W., Barry, P.H. 1996. Calcium-dependent modulation of the agonist affinity of the mammalian olfactory cyclic nucleotide-gated channel by calmodulin and a novel endogenous factor. *J. Membrane Biol.* **152:**13–23

Barry, P.H. 1994. JPCalc, a software package for calculating liquid junction potential corrections in patch-clamp, intracellular, epithelial and bilayer measurements and for correcting junction potential measurements. *J. Neurosci. Methods* **51:**107–116

Belluscio, L., Gold, G.H., Nemes, A., Axel, R. 1998. Mice deficient in G_{olf} are anosmic. *Neuron* **20:**69–81

Boekhoff, I., Michel, W.C., Breer, H., Ache, B.W. 1994. Single odors differentially stimulate dual second-messenger pathways in lobster olfactory receptor cells. *J. Neurosci.* **14:**3304–3309

Bönigk, W., Bradley, J., Müller, F., Sesti, F., Boekhoff, I., Ronnett, G.V., Kaupp, U.B., Frings, S. 1999. The native rat olfactory cyclic nucleotide-gated channel is composed of three distinct subunits. *J. Neurosci.* **19:**5332–5347

Breer, H., Boekhoff, I., Tareilus, E. 1990. Rapid kinetics of second messenger formation in olfactory transduction. *Nature* **345:**65–68

Brunet, L.J., Gold, G.H., Ngai, J. 1996. General anosmia caused by a targeted disruption of the mouse olfactory cyclic nucleotide-gated cation channel. *Neuron* **17:**681–693

Buck, L., Axel, R. 1991. A novel multigene family may encode odorant receptors: a molecular basis for odor recognition. *Cell* **65:**175–187

Ehrlich, B.E., Watras, J. 1988. Inositol 1,4,5-trisphosphate activates a channel from smooth muscle sarcoplasmic reticulum. *Nature* **336:**583–586

Fadool, D.A., Ache, B.W. 1992. Plasma membrane inositol 1,4,5-trisphosphate-activated channels mediate signal transduction in lobster olfactory receptor neurons. *Neuron* **9:**907–918

Firestein, S., Werblin, F. 1987. Gated currents in isolated olfactory receptor neurons of the larval tiger salamander. *Proc. Natl. Acad. Sci. USA* **84:**6292–6296

Firestein, S., Zufall, F., Shepherd, G.M. 1991. Single odor-sensitive channels in ORNs are also gated by cyclic nucleotides. *J. Neurosci.* **11:**3565–3572

Frings, S., Seifert, R., Godde, M., Kaup, U.B. 1995. Profoundly different calcium permeation and blockage determine the specific function of distinct cyclic nucleotide-gated channels. *Neuron* **15:**169–179

Gold, G.H. 1999. Controversial issues in vertebrate olfactory transduction. *Annu. Rev. Physiol.* **61:**857–871

Goulding, E.H., Ngai, J., Kramer, R.H., Colicos, S., Axel, R., Siegelbaum, S., Chess, A. 1992. Molecular cloning and single-channel properties of the CNG-gated channel from catfish ORNs. *Neuron* **8:**45–58

Hamill, O.P., Marty, A., Neher, E., Sakmann, B., Sigworth, F.J. 1981. Improved patch-clamp techniques for high resolution current recording from cells and cell-free membrane patches. *Pfluegers. Arch. Eur. J. Physiol.* **391:**85–100

Hatt, H., Ache, B.W. 1994. Cyclic nucleotide- and inositol phosphate-gated ion channels in lobster olfactory receptor neurons. *Proc. Natl. Acad. Sci. USA* **91:**6264–6268

Hille, B. 1984. Ionic Channels of Excitable membranes. Sinauer, Massachusetts.

Honda, E., Teeter, J.H., Restrepo, D. 1995. IP_3-gated ion channels in rat olfactory cilia membrane. *Brain Res.* **703:**79–85

Huque, T., Bruch, R.C. 1986. Odorant- and guanine nucleotide stimulated phosphoinositide turnover in olfactory cilia. *Biochem. Biophys, Res. Commun.* **137:**36–42

Kalinoski, D.L., Aldinger, S.B., Boyle, A.G., Huque, T., Marecek, J.F., Prestwich, G.D., Restrepo, D. 1992. Characterization of a novel inositol 1,4,5-trisphosphate receptor in isolated olfactory cilia. *Biochem. J.* **281:**449–456

Kashiwayanagi, M. 1996. Dialysis of inositol 1,4,5-trisphosphate induces inward currents and Ca^{2+} uptake in frog olfactory receptor cells. *Biochem. Biophys. Res. Commun.* **225:**666–671

Kaur, R., Moorhouse, A.J., Barry, P.H. 1999. IP_3-gated channels in excised membrane patches from the soma and dendritic knob of rat ORNs. *Proc. Aust. Physiol. Pharmacol. Soc.* **30:**9P (Abstr.)

Kleene, S.J. 1993. Origin of the chloride current in olfactory transduction. *Neuron* **11:**123–132

Kleene, S.J., Gesteland, R.C. 1991. Calcium-activated chloride conductance in frog olfactory cilia. *J. Neurosci.* **11:**3624–3629

Kleene, S.J., Gesteland, R.C., Bryant, S.H. 1994. An electrophysiological survey of frog olfactory cilia. *J. Exp. Biol.* **195:**307–328

Kurahashi, T., Kaneko, A. 1991. High density cAMP-gated channels at the ciliary membrane in the olfactory receptor cell. *NeuroReport.* **2:**5–8

Kurahashi, T., Kaneko, A. 1993. Gating properties of the cAMP-gated channel in toad olfactory receptor cells. *J. Physiol.* **466:**287–302

Kurahashi, T., Yau, K.W. 1993. Co-existence of cationic and chloride components in odorant-induced current of vertebrate olfactory receptor cells. *Nature* **363:**71–74

Lischka, F.W., Zviman, M. Teeter, J.H., Restrepo, D. 1999. Characterization of IP_3-gated channels in the plasma membrane of rat ORNs. *Biophy. J.* **76:**1410–1422

Lowe, G., Gold, G.H. 1993a. Contribution of the ciliary cyclic nucleotide-gated conductance to olfactory transduction in the salamander. *J. Physiol.* **462:**175–196

Lowe, G., Gold, G.H. 1993b. Nonlinear amplification by calcium-dependent chloride channels in olfactory receptor cells. *Nature* **366:**283–286

Lynch, J.W., Barry, P.H. 1989. Action potentials initiated by single channel openings in a small neuron (rat olfactory receptor). *Biophys. J.* **55:**755–768

Lynch, J.W., Barry. P.H. 1991. Properties of transient K^+ currents and underlying single K^+ channels in rat ORNs. *J. Gen. Physiol.* **97:**1043–1072

Miyamoto, T., Restrepo, D., Cragoe, Jr., E.J., Teeter, J.H. 1992. IP_3- and cAMP-induced responses in isolated olfactory receptor neurons from the channel catfish. *J. Membrane Biol.* **127:**173–183

Nakamura, T., Gold, G.H. 1987. A cyclic nucleotide-gated conductance in olfactory receptor cilia. *Nature* **325:**442–444

Nakamura, T., Lee, H.H., Kobayashi, H., Satoh, T.O. 1996. Gated conductances in native and reconstituted membranes from frog olfactory cilia. *Biophys. J.* **70:**813–817

Noé, J., Breer, H. 1998. Functional and molecular characterization of individual olfactory neurons. *J. Neurochem.* **71:**2286–2293

Okada, Y., Teetet, J.H., Restrepo, D. 1994. Inositol 1,4,5-trisphosphate-gated conductance in isolated rat olfactory neurons. *J. Neurophysiol.* **71:**595–602

Restrepo, D. 1992. Characterization of a novel inositol 1,4,5-trisphosphate receptor in isolated olfactory cilia. *Biochem. J.* **281:**449–456

Restrepo, D., Miyamoto, T., Bryant, B.P., Teeter, J.H. 1990. Odor stimuli trigger influx of calcium into olfactory neurons of the channel catfish. *Science* **249:**1166–1168

Restrepo, D., Teeter, J.H., Honda, E., Boyle, A.G., Mareck, J.F., Prestwich, G.D., Kalinoski, D.L. 1992. Evidence for an IP_3-gated channel protein in isolated rat olfactory cilia. *Am. J. Phys.* **263:**C667–C673

Restrepo, D., Teeter, J.H., Schild, D. 1996. Second messenger signaling in olfactory transduction. *J. Neurobiol.* **30:**37–48

Schild, D., Lischka, F.W., Restrepo, D. 1995. $InsIP_3$ causes an increase in apical $[Ca^{2+}]_i$ by activating two distinct components in vertebrate olfactory receptor cells. *J. Neurophysiol.* **73:**862–866

Schild, D., Restrepo, D. 1998. Transduction mechanisms in vertebrate olfactory receptor cells. *Physiol. Rev.* **78:**429–466

Suzuki, N. 1994. IP_3-activated ion channel activities in olfactory receptor neurons from different vertebrate species. *In* Olfaction and Taste X1. K. Kurihara, N. Suzuki, and H. Ogawa, eds. Springer-Verlag, Tokyo. 173–177

Vogl, A., Noë, J., Breer, H., Boekhoff, I. 2000. Cross-talk between olfactory second messenger pathways. *Eur. J. Biochem.* **267:**4529–4535